ChemEngineering

MDPI

Article

Effect of Alkyl Chain Length of Quaternary Ammonium Surfactant Corrosion Inhibitor on Fe (110) in Acetic Acid Media via Computer Simulation

Mohd Sofi Numin [1], Khairulazhar Jumbri [1,*], Kee Kok Eng [2], Almila Hassan [3], Noorazlenawati Borhan [4], Nik M. Radi Nik M. Daud [4], Azmi M. Nor A [4], Firdaus Suhor [4] and Nur Nadia Dzulkifli [5]

[1] Department of Fundamental and Applied Sciences, Universiti Teknologi PETRONAS, Seri Iskandar 32610, Perak, Malaysia; mohd_22009501@utp.edu.my
[2] Department of Mechanical Engineering, Universiti Teknologi PETRONAS, Seri Iskandar 32610, Perak, Malaysia; keekokeng@utp.edu.my
[3] Centre for Foundation Studies, Universiti Teknologi PETRONAS, Seri Iskandar 32610, Perak, Malaysia; almila.hassan@utp.edu.my
[4] PETRONAS Research Sdn Bhd, Bandar Baru Bangi 43000, Selangor, Malaysia; noorazlenawati_borhan@petronas.com (N.B.); radi.daud@petronas.com (N.M.R.N.M.D.); azminr@petronas.com (A.M.N.A.); mfirdaus_suhor@petronas.com (F.S.)
[5] Faculty of Applied Sciences, Kuala Pilah Campus, Universiti Teknologi MARA (UITM), Shah Alam 40450, Selangor, Malaysia; nurnadia@uitm.edu.my
* Correspondence: khairulazhar.jumbri@utp.edu.my; Tel.: +60-53687843

Abstract: Density functional theory (DFT) and molecular dynamics (MD) simulations were employed to investigate the inhibition mechanism of cationic quaternary ammonium surfactant corrosion inhibitors (CIs) with varying chain lengths in 1.0 M HCl and 500 ppm acetic acid on Fe (110) surfaces. DFT calculations demonstrated that all surfactant CI molecules possess favorable inhibition properties, with the cationic quaternary ammonium groups (N^+) and alpha carbon serving as electron-donating reactive centers, characterized by a low band-gap energy of 1.26 eV. MD simulations highlighted C12, with a 12-alkyl chain length, as the most promising CI molecule, exhibiting high adsorption and binding energies, a low diffusion coefficient, and a random distribution at low concentrations, thereby facilitating optimal adsorption onto the Fe (110) metal surface. The insights gained from computational modeling regarding the influence of alkyl chain length on inhibition efficiency, coupled with the comprehensive theoretical understanding of cationic quaternary ammonium surfactant CI molecules in acidic corrosion systems, can serve as a foundation for the future development of innovative surfactant CI molecules incorporating ammonium-based functional groups.

Keywords: corrosion inhibitor; quaternary ammonium; MD simulation; DFT calculation; adsorption

check for updates

Academic Editor: Vincenzo Russo

Received: 14 November 2024
Revised: 16 December 2024
Accepted: 31 December 2024
Published: 8 January 2025

Citation: Numin, M.S.; Jumbri, K.; Eng, K.K.; Hassan, A.; Borhan, N.; Daud, N.M.R.N.M.; A, A.M.N.; Suhor, F.; Dzulkifli, N.N. Effect of Alkyl Chain Length of Quaternary Ammonium Surfactant Corrosion Inhibitor on Fe (110) in Acetic Acid Media via Computer Simulation. *ChemEngineering* **2025**, *9*, 7. https://doi.org/10.3390/chemengineering9010007

1. Introduction

Corrosion is defined as degradation of materials, with consequent diminution of their properties, due to deteriorative interactions with environments to which they are exposed [1]. The environments that are usually exposed to pipelines that can enhance the corrosion rate are corrosive media such as dissolved H_2S, Cl_2, O_2, and CO_2. Another environment faced by pipelines in petroleum industries is organic acid condition. The presence of organic acid increases the solubility of corrosion product films, leading to the reduction in protective corrosion products. The presence of these acids will increase the

hydrogen concentration and the acidic environment that favors the corrosion attack towards the metal surface. Among all organic acids, acetic acid is the most abundant, produced by the reaction between hydrocarbons in crude oil, water molecules, and chemicals used to enhance the oil recovery process [2,3].

Corrosion-resistant alloys (CRAs), protective coatings, corrosion inhibitors, and cathodic protection are commonly employed in the petroleum industry to control corrosion. While CRAs and corrosion inhibitors are effective in reducing internal corrosion caused by corrosive fluids, which can lead to the degradation of processing equipment and pipelines, corrosion inhibitors are widely regarded as a highly economical and efficient method for mitigating internal corrosion [4]. A review by Xiong et al. [5] has stated that the surfactant molecules can perform as corrosion inhibitors due to their high affinity to adsorb over the interface, resulting in a higher potential in resolving corrosion issues over metal surfaces. Verma et al. [6] also stated that the corrosion inhibition performance of surfactants is based on the surfactant molecules' adsorption capacity over the metal surface's reactive sites. Cationic quaternary ammonium surfactant is a surfactant compound that contains a hydrophilic head (N^+) and a hydrophobic tail (alkyl chain) that is an excellent corrosion inhibitor due to its properties that could be adsorbed on the metal surface and form a protective layer [7]. The strong adsorption of nitrogen atoms from the cationic quaternary ammonium surfactant molecules on the metal surface leads to the formation of an adsorption film that separates the metal from the corrosive medium [8]. In 2021, Abdellaoie et al. [9] found that cationic quaternary ammonium surfactant, namely, 12-(2, 3-dioxoindolin-1-yl)-N,N,N-trimethyldodecanammonium bromide, has a higher inhibition efficiency (95.9%) at a concentration of 1.0 mM in the presence of 1.0 M HCl at a temperature of 298 K. Moreover, Alnajjar et al. [10] synthesized N,N-dimethyl-N-(3-((2-nitrophenyl)sulfonamido)propyl)dodecan-1-aminium iodide, another cationic quaternary ammonium surfactant, and found that this surfactant was able to increase the inhibition efficiency up to 98.6% in the presence of 15% HCl solution. Numin et al. (2022) highlighted the prevalence of cationic quaternary ammonium (N^+) as a key functional group in surfactant inhibitor design [11]. Thus, developing novel surfactant inhibitors using N^+ as a headgroup could offer significant potential for corrosion mitigation.

Adsorption is critical for the inhibitory activity of surfactant-based corrosion inhibitors. Numin et al. emphasized the importance of understanding adsorption properties for elucidating inhibition mechanisms [11]. Computational simulations, including DFT and MD, can provide valuable insights into these properties. For instance, Zhu et al. (2021) demonstrated that Gemini surfactant 10-12-10, predicted to have lower bandgap energy and higher adsorption energy, exhibited superior corrosion inhibition compared to its monomeric counterpart 1227 [12]. This correlation between computational predictions and experimental observations underscores the potential of computational simulations for screening and predicting surfactant inhibitor performance. In 2019, Gao et al. studied the effect of the alkyl chain of cationic quaternary ammonium cationic surfactants on corrosion inhibition in HCl solution experimentally. They found that the dodecyl trimethyl ammonium chloride (DTAC) performed the best with the highest inhibition efficiency of >90% [7]. However, the in-depth study on the adsorption mechanism of cationic quaternary ammonium cationic surfactants by computer simulation methods is limited. The previous researchers only focused on the strong acidic conditions such as HCl, sulfuric acid (H_2SO_4), and phosphoric acid (H_3PO_4), and there is a lack of studies in acetic acid (CH_3COOH) conditions, which are more applicable in the petrochemical industries' pipelines. Thus, this study focuses on the adsorption mechanism of cationic quaternary ammonium surfactants with varying alkyl chain lengths (C10, C12, C14, C16, and C18) on Fe(110) surfaces in the presence of HCl and acetic acid, using DFT calculations and MD simulations.

2. Materials and Methods

2.1. Density Functional Theory (DFT) Calculation

DFT calculations offer a rapid and reliable method for predicting the electronic properties of corrosion inhibitors, enabling theoretical analysis of their electronic structures [13]. A compound's electronic properties directly influence the adsorption behavior of ammonium surfactant cationic CIs on metal surfaces. Using the TmoleX software 4.0, DFT calculations were performed on ammonium surfactant CIs with varying alkyl chain lengths (C10, C12, C14, C16, and C18). These calculations employed the hybrid B3LYP functional [14,15] and the def-SV(P).h basis set [16,17] in a non-aqueous, vacuum environment. The input file was generated for ground-state calculations under DFT settings, and the resulting parameters were visualized and analyzed using the TmoleX program.

The output parameters calculated include the highest occupied molecular orbital energy (E_{HOMO}) and the lowest unoccupied molecular orbital energy (E_{LUMO}). Then, both HOMO and LUMO energy were used to calculate the other inhibition parameters of ammonium surfactant cationic CI molecules, such as band-gap energy (ΔE), number of transferred electrons (ΔN), electronegativity (χ), hardness (η), softness (σ), ionization potential (I), and electron affinity (A). The derived output parameters, equation, description, and reference are tabulated in Table 1.

Table 1. The output parameters, equations, descriptions, and references for the DFT calculation.

Parameters	Equation	Description	Reference
E_{HOMO}	From DFT	Ability to donate electrons	[18]
E_{LUMO}	From DFT	Ability to accept electrons	[18]
ΔE	$\Delta E = E_{LUMO} - E_{HOMO}$	Reactivity of the molecules	[18]
I	$I = -E_{HOMO}$	Ability to donate electrons	[19]
A	$A = -E_{LUMO}$	Ability to accept electrons	[19]
χ	$\chi = \frac{I+A}{2}$	Ability to attract electrons	[20]
η	$\eta = \frac{I-A}{2}$	Resistance towards the deformation of electron cloud around the molecules	[20]
σ	$\sigma = \frac{1}{\eta}$	Capacity of an atom or groups of atoms to receive electrons	[21]
ΔN	$\Delta N = \frac{\chi_{Fe}-\chi_{inh}}{2(\eta_{Fe}+\eta_{inh})}$	The number of electron transfers from molecules to metal surfaces	[22,23]

2.2. Molecular Dynamics (MD) Simulation

MD simulations have been employed to investigate the molecular-level interactions between corrosion inhibitors and corrosion systems in the presence of acetic acid. These simulations can provide insights into the molecular orientation of CI molecules on metal surfaces, the strength of adsorption, and the aggregation behavior of CI molecules at various concentrations [24]. The initial coordinates of C10, C12, C14, C16, and C18 CI molecules were submitted to the Automated Topology Builder (ATB) and Repository Version 3.0 server to obtain optimized geometric, chemical, and topological information. The metal surface used in this simulation was Fe (110) because it is a densely packed surface and, therefore, the most stable [25]. In the adsorption energy (E_{ads}) and binding energy (E_{bind}) calculation, each CI molecule filled the center of the box with a size of 51.60, 51.60, and 77.40 Å. The Fe (110) and the acidic medium were added into the box that contained hydronium ion (H_3O^+), chloride ion (Cl^-), water (H_2O), and acetic acid molecules. Figure 1 shows the corrosion system without the presence of a CI molecule. For molecular aggregation analysis, the systems were constructed at five different concentrations of CI molecules (0.04, 0.08, 0.12, 0.16, and 0.20 M).

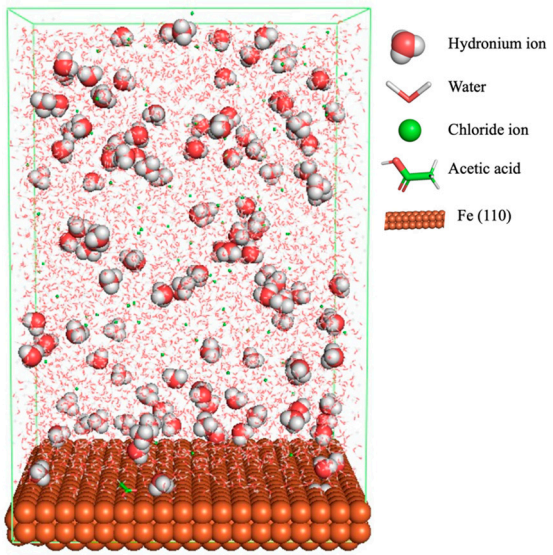

Figure 1. The corrosion system of Fe (110) as a metal in 1.0 M HCl and 500 ppm acetic acid.

After system preparation, the MD simulation commenced with energy minimization using the steepest descent and conjugate gradient methods for 5000 steps. This step resolved atomic collisions, bond distortions, and other unfavorable interactions, resulting in a more stable initial structure for the simulation. Subsequently, the simulation proceeded with a 5 ns canonical (NVT) ensemble followed by a 5 ns isothermal–isobaric (NPT) ensemble. The NVT ensemble established the appropriate system temperature for calculating adsorption energy, while the NPT ensemble allowed for the investigation of molecular aggregation at different temperatures. Periodic boundary conditions (PBCs) were applied in all directions (x, y, and z) with a 2.0 fs time step. Electrostatic interactions were calculated using the Particle Mesh Ewald (PME) method [26] with a grid spacing of 0.12 nm and fourth-order interpolation. Coulomb and Lennard–Jones interactions were summed up to 1.2 nm, and the neighbor list with a cutoff of 1.2 nm was updated every five steps. Bond lengths for solute and organic solvent molecules were constrained using the LINCS algorithm [27], while the SETTLE algorithm was employed for water molecules [28]. The GROMACS software package version 4.5 with the GROMOS force field was utilized throughout the simulation (see Tables S1–S5 Supplementary Material the partial atomic charges for all CI molecules).

3. Results and Discussion

3.1. Density Functional Theory (DFT) Calculation

DFT calculations can elucidate the adsorption properties of CI molecules on metal surfaces. The HOMO, localized on the cationic quaternary ammonium groups of CI molecules, represents electron-donating sites that can interact with the empty 3d-orbitals of iron (Fe) atoms. Conversely, the LUMO, located on the alpha carbon, represents electron-accepting sites capable of back-donation from the metal surface [29,30]. Table 2 illustrates the optimized structures, HOMOs, and LUMOs of all CI molecules. The cationic quaternary ammonium groups, characterized by both polar (N^+) and non-polar (alkyl) termini, exhibit good electrolyte properties and strong adsorption tendencies [31]. The HOMO distribution on these groups facilitates electron donation to the Fe 3d-orbitals. Additionally, for C10, C14, and C16, the alpha carbon, acting as a LUMO site, can engage in back-donation with the Fe atoms, further enhancing adsorption. The cationic nature of the nitrogen atom in the quaternary ammonium groups promotes physisorption, a charge-based interaction that hinders chloride anion attack on the Fe surface, thus inhibiting the anodic iron oxidation

reaction [32]. However, the study by Abdellaoui et al. in 2021 demonstrated that the adsorption of cationic quaternary ammonium surfactants onto metal surfaces can involve both physisorption and chemisorption, also called mixed inhibitors [9]. Chemisorption occurs through the formation of covalent bonds, with electron transfer from the nitrogen cation and alpha carbon of the cationic quaternary ammonium surfactant to the vacant *d*-orbital of the metal surface. Alternatively, a back-donation mechanism can transfer electrons from the metal d-orbital to the carbon adjacent to the cationic quaternary ammonium surfactant region (Figure 2).

Table 2. Optimized structures, HOMO, and LUMO of ammonium surfactant CI molecules.

CI Molecule	Optimized	HOMO	LUMO
C10	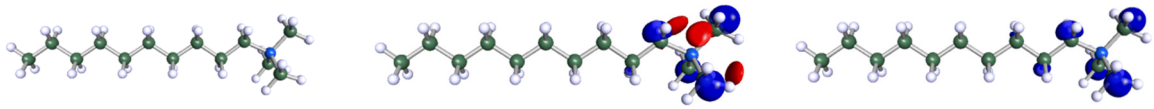		
C12	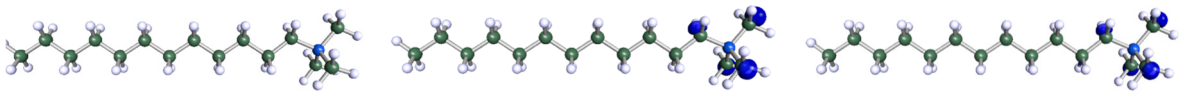		
C14	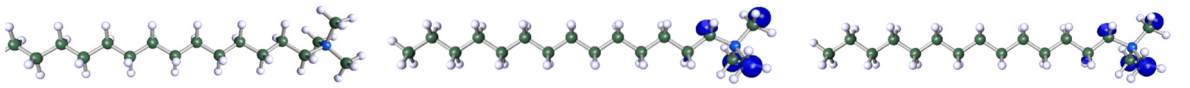		
C16	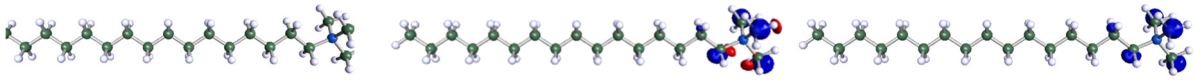		
C18	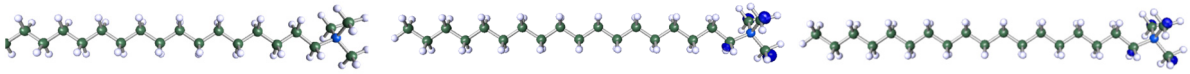		

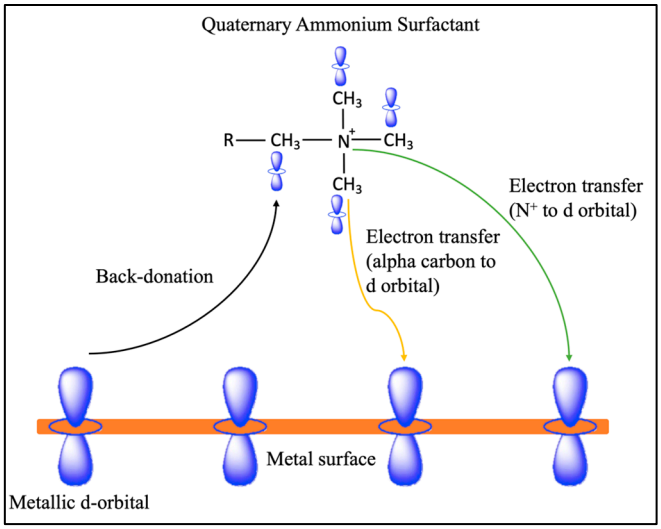

Figure 2. Mechanism of physisorption and chemisorption of the cationic quaternary ammonium surfactant CI molecule on the metal surface.

The output parameters derived from the DFT calculation are tabulated in Table 3. The adsorption ability as a donor–acceptor contributor of CI molecules is depicted by the energy of HOMO (E_{HOMO}) and LUMO (E_{LUMO}). The higher value of E_{HOMO} implies the higher donor ability, while the higher value of E_{LUMO} represents the acceptor ability of the CI molecules. The band gap energy, ΔE, is the difference between LUMO energy and

HOMO energy, where the lower ΔE value for all CI molecules (1.26 eV) indicates the higher reactivity of the CI molecules as a donor–acceptor contributor. The identical band gap energy values observed among all cationic quaternary ammonium surfactant CI molecules with varying alkyl chain lengths indicated that the reactivity of these molecules is primarily determined by their reactive HOMO and LUMO regions. This finding is attributed to the quantum chemical DFT calculations, which were performed on individual CI molecules without considering any solvent effects. Consequently, the alkyl chain length exerts a minimal influence on the band gap energy. However, the alkyl chain can play a crucial role in molecular adsorption by providing steric hindrance and protecting the reactive region from interactions with other molecules. This aspect will be explored further in the subsequent section on MD simulation methods. The illustration of the HOMO, LUMO, and ΔE for the C10 molecule is shown in Figure 3.

Table 3. Calculated DFT calculation parameters of all cationic quaternary ammonium cationic surfactant CI molecules.

CI Molecule	E_{HOMO} (eV)	E_{LUMO} (eV)	ΔE (eV)	Ionization Potential, I	Electron Affinity, A	Global Hardness, η	Electronegativity, χ	Softness, σ	Fraction of Transferred Electron, ΔN
C10	−0.2911577	0.9714327	1.2625904	0.2911577	−0.9714327	0.6312952	−0.3401375	1.584045	5.813554024
C12	−0.2911577	0.9687116	1.2598693	0.2911577	−0.9687116	0.62993465	−0.33877695	1.587466	5.825030382
C14	−0.2911577	0.9687116	1.2598693	0.2911577	−0.9687116	0.62993465	−0.33877695	1.587466	5.825030382
C16	−0.2857155	0.9741538	1.2598693	0.2857155	−0.9741538	0.62993465	−0.34421915	1.587466	5.829350037
C18	−0.2911577	0.9687116	1.2598693	0.2911577	−0.9687116	0.62993465	−0.33877695	1.587466	5.825030382

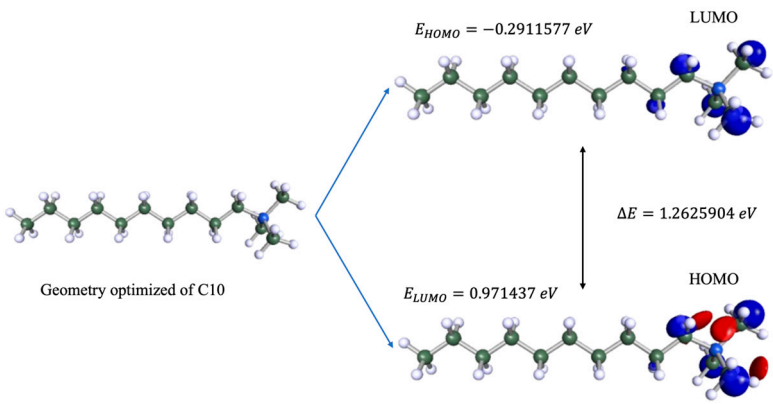

Figure 3. Geometrically optimized structure of C10 structure, HOMO, LUMO, and bandgap energy value illustration.

A study by Han et al. [12] has proven experimentally that the CI molecule with the lowest ΔE value gave the highest efficiency as a corrosion inhibitor compared to CI molecules that have a higher ΔE value. The HOMO and LUMO energy values also affect the electronegativity (χ), hardness (η), and softness (σ) of the CI molecules. All CI molecules have a low χ value, which indicates the higher ability of the molecules to donate electrons. The low value of η and high σ value also show the higher reactivity of the CI molecules in the electron transfer process [33]. The final output parameter is the number of transferred electrons from CI molecules (ΔN). The positive value of ΔN indicates that the major electron transfer process is from CI molecules to the iron metal surfaces [34,35]. The electron-donating ability of these CI molecules is due to the HOMO that is distributed at the alpha carbon regions of the molecules, representing the ability to donate electrons compared to the LUMO that is only circulated at the next carbon from the alpha carbon. DFT calculations have shown that cationic quaternary ammonium surfactant CI molecules can act as both nucleophiles and electrophiles. These molecules can

donate electrons to metal surfaces and receive electrons through back-donation, forming coordination bonds via chemisorption. Moreover, the cationic nature of nitrogen allows for physisorption through charge interaction with the metal surface [7]. The length of the alkyl group attached to the cationic quaternary ammonium surfactants does not significantly influence the electron-donating ability of the CI molecules, as indicated by the minimal variation in the DFT-derived parameters. To assess the impact of alkyl chain length on corrosion inhibition efficiency, the polarity and solubility of the compounds must also be considered. Due to the inverse relationship between alkyl chain length and both polarity and solubility, shorter alkyl chains generally correlate with improved corrosion inhibition performance [36]. The effects of polarity and solubility will be further explored in the MD simulation analysis with the presence of the corrosion solution.

3.2. Molecular Dynamics (MD) Simulation

3.2.1. Adsorption Properties of CI Molecules

The MD simulation was used to study the adsorption behavior and the interaction of CI molecules (C10, C12, C14, C16, and C18) towards the Fe (110) metal surface in the presence of 1.0 M HCl and 500 ppm acetic acid solution. The addition of HCl and acetic acid solution is to increase the corrosion attack towards the metal surface. Figure 4 shows the top and side view of the CI molecule on the Fe (110) surface after MD simulation. The molecules behaved as if they were in a planar orientation on the Fe (110) surface, which is more favorable towards the inhibition due to the mechanism of CI that should form a film formation to cover the metal surface from the corrosion attack. The CI with planar orientation will cover more surface than the horizontal orientation. Moreover, horizontal orientation will also reduce the adsorption strength of its reactive site due to the hydrophobic part that will undergo force of interaction with the bulk corrosion solution [37]. Theoretically, in the horizontal orientation, longer alkyl chains on CI molecules experience greater shear forces, which can disrupt the adsorption of the CI molecules' reactive regions to the metal surface. Figure 4 demonstrates the adsorption of the cationic quaternary ammonium group onto the metal surface, accompanied by charge interactions and electron transfer between the reactive region of the CI molecules and the metal. This observation aligns with the DFT calculation results, which identified the cationic quaternary ammonium and alpha carbon regions as the HOMO with a high electron-donating capacity. On the other hand, the hydrophobic side of the surfactant molecules is also attached to the metal surface due to the electron back donation from the Fe atom to the alkyl group of the CI molecule [37]. According to El Defrawy et al. in 2019, the back-donation ability of the CI molecules is directly proportional to the hardness (η), as defined in the following Equation (1) [38]:

$$\Delta E_{back-donation} = \frac{-\eta}{4} \tag{1}$$

where $\Delta E_{back-donation}$ is the band-gap energy for the back-donation mechanism. The $\Delta E_{back-donation}$ value is tabulated in Table 4 and shows that the values of $\eta > 0$ and $\Delta E_{back-donation} < 0$ imply that back-donation from the metal to the CI molecule is energetically favored [39,40]. C12, C14, C16, and C18 have the highest back donation ability with the same $\Delta E_{back-donation}$ value of -0.1574837 eV, compared to the C10 CI molecule with a $\Delta E_{back-donation}$ value of -0.1578238 eV. As the LUMO region resides within the alkyl groups, increasing the alkyl chain length by two carbons beyond the shortest inhibitor, C10, to C12, enhances back-donation capability. C12 represents the optimal value for back-donation, with the corresponding value remaining relatively constant up to C18. Back-donation is also called the back-bonding mechanism, where the carbon atom in the CI molecule can accept electrons back from the metal to strengthen the bond between the

metal and the carbon of the CI molecule [41]. The results show that the cationic quaternary ammonium CI with a longer alkyl chain length provides a site for the back donation mechanism from the Fe metal.

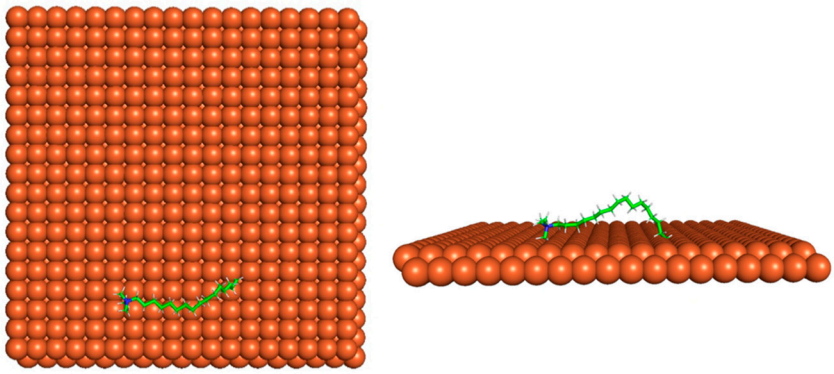

Figure 4. Top and side view of the CI molecule after MD simulation. The H_3O^+, Cl^-, and H_2O molecules were removed for clarification.

Table 4. Global hardness and $\Delta E_{back-donation}$ values of all CI molecules after DFT calculation.

CI Molecules	Global Hardness (η), eV	$\Delta E_{back-donation}$, eV
C10	0.6312952	−0.1578238
C12	0.62993465	−0.1574837
C14	0.62993465	−0.1574837
C16	0.62993465	−0.1574837
C18	0.62993465	−0.1574837

3.2.2. Adsorption Energy

Three different systems were constructed, and the energy of all systems was calculated to find the adsorption energy at seven different temperatures (303, 313, 323, 333, 343, 353, and 363 K). The systems include the corrosion system with CI molecules, the corrosion system without CI molecules, and CI molecules only. Equation (2) was used to calculate the adsorption energy (E_{ads}) [33].

$$E_{ads} = E_{total} - \left(E_{surface+solution} + E_{inhibitor}\right) \quad (2)$$

where E_{total} is the energy for corrosion in a system with CI molecules, $E_{surface+solution}$ is the energy for a corrosion system without CI molecules, and $E_{inhibitor}$ is the energy of the system with CI molecules only. Figure 5 shows the plot of calculated adsorption energy for all CI molecules in the acidic corrosion system at different temperatures. The negative value of adsorption energy for all systems indicates the spontaneity of the adsorption process between CI molecules and the Fe (110) metal surface. The higher the negative value of adsorption energy denotes, the stronger the adsorption [24]. Another energy parameter that can describe the inhibition of CI molecules is binding energy (E_{bind}). The E_{bind} value can be translated from the adsorption energy and can be calculated using Equation (3):

$$E_{ads} = -E_{bind} \quad (3)$$

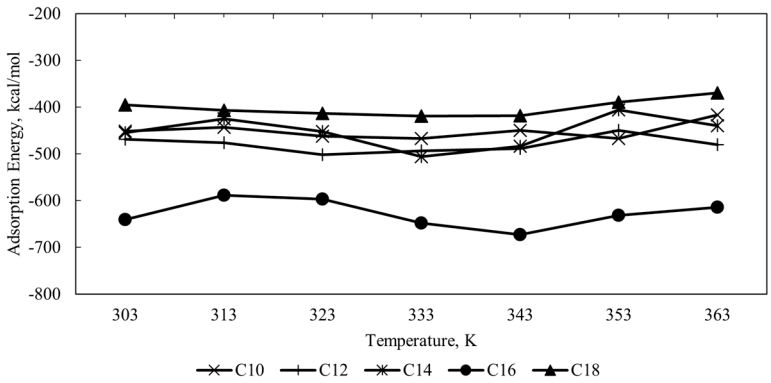

Figure 5. The adsorption energy of corrosion inhibitors at different alkyl chain lengths at different temperatures between 298 and 363 K.

The E_{ads} and E_{bind} values for all molecules at temperature 323 K were tabulated in Table 5, where the E_{bind} value for all molecules is positive, indicating its tendency to the adsorption process. The order of binding energy for all molecules is as follows: C16 > C12 > C10 > C14 > C18. Binding energy is referred to as the attraction forces between the CI molecules and the metal surfaces. For the cationic quaternary ammonium surfactant CI molecules, the attraction forces mainly happen due to the ionic properties of the hydrophilic head and the hydrophobic interaction of the hydrophobic tail in the bulk solution of the corrosion system [37,42]. The results show that CI molecules' adsorption and binding energy values vary with different alkyl chain lengths. Among all the CI molecules, C18, with the longest alkyl chain, exhibits the weakest adsorption strength. Conversely, C16, with the second-longest alkyl chain, demonstrates the strongest adsorption strength, adsorption magnitude, and binding energy. The alkyl chain length significantly influences the adsorption strength of CI molecules onto the Fe (110) metal surface, with longer chains generally leading to stronger adsorption. Extended alkyl chains effectively shield the positively charged nitrogen and alpha carbon of the cationic quaternary ammonium surfactant from the shear and flow effects of the bulk corrosion solution. This is attributed to the increased number of carbon atoms in longer chains, which can interact through van der Waals forces, promoting aggregation among the alkyl chains rather than their interaction with the surface. Additionally, the greater conformational freedom of longer chains can hinder their ability to adopt the specific conformations required for strong adsorption. Furthermore, longer alkyl chains can create steric hindrance, limiting the molecules' proximity to the metal surface and reducing the effective contact area, thereby decreasing adsorption strength. The longer the alkyl chain length, the more the hydrophobic group that extends away from the interface towards the solution and provides further protection by forming an array of hydrophobic tails, resulting in the change of electrochemical behavior of the metal [43,44]. Hence, the binding energy between the reactive regions (HOMO and LUMO) of the corrosion inhibitor molecule with the Fe metal surface increases as the alkyl chain length increases.

Table 5. The adsorption energy and binding energy of corrosion inhibitors with different alkyl chain lengths at 323 K.

CI Molecules	Adsorption Energy, E_{ads} (kcal/mol)	Binding Energy, E_{bind} (kcal/mol)
C10	−461.88	461.88
C12	−501.59	501.59
C14	−452.01	452.01
C16	−597.12	597.12
C18	−413.12	413.12

However, there are some cases where adding alkyl chain length reduces the adsorption strength of the reactive site of the CI molecule towards the metal surface. The decrease in adsorption may be due to the shear and the flow effect experienced by the extended hydrophobic alkyl chain from the bulk solution. The results show a fluctuation of the adsorption strength as the alkyl chain length extended. Hence, the optimum value of the alkyl chain length is required to be explicitly investigated due to the variation effect of the adsorption strength on the alkyl chain length of the cationic quaternary ammonium surfactant CI molecules on the Fe (110) metal surface, where in this case the highest adsorption is C16, followed by C12, C10, C14, and C18 molecules.

3.2.3. Molecular Aggregation

To investigate molecular aggregation, five systems were constructed for each CI molecule at different concentrations (0.04, 0.08, 0.12, 0.16, and 0.20 M) in the presence of 1.0 M HCl, 500 ppm acetic acid, and a temperature of 333 K. To focus solely on molecular aggregation in the bulk solution containing corrosion particles, the Fe (110) metal surface was excluded from these systems. Figure 6 illustrates the constructed system. The molecular behavior of the CI molecules was analyzed based on their diffusion towards the bulk solution or corrosion particles. The diffusion coefficient, defined as the quantity of a substance diffusing through a unit cross-sectional area per unit time under a unit concentration gradient, was calculated using Einstein's diffusion equations (Equations (4) and (5)) [45,46].

$$MSD = \left\{ [R_i(t) - R_i(0)]^2 \right\} \tag{4}$$

$$D = \frac{1}{6N_a} \sum_{i=1}^{N} \left\{ [R_i(t) - R_i(0)]^2 \right\} \tag{5}$$

where t is the time, $R_i(t)$ is the position vector of molecule i at time t, and N is the number of diffusing molecules. The mean square displacement (MSD) was derived from the MD simulation, and the limiting slope of the MSD as a function of time can be used to determine the diffusion coefficient of a molecule [47]. As shown in Figure 7, the diffusion coefficient of CI molecules towards corrosion particles decreases with increasing alkyl chain length. The increased hydrophobicity of longer alkyl chains hinders their diffusion towards polar corrosion particles, creating a diffusion barrier that promotes adsorption onto the metal surface and strengthens the metal–inhibitor interaction [48]. As noted by Obot et al. [47], a low diffusion coefficient of CI molecules indicates promising inhibitory capacity against the diffusion of corrosion particles. Their findings, supported by experimental data, demonstrate that CI molecules with the lowest diffusion coefficient exhibit the highest inhibition efficiency.

The diffusion coefficient of all CI molecules correlated with their aggregation behavior in the corrosion system. A decrease in diffusion was associated with rapid aggregation and cluster formation [25,49]. According to Sharma et al. [49], clustered CI molecules exhibit weaker adsorption on metal surfaces compared to randomly dispersed molecules. Table 6 presents the aggregation behavior of all CI molecules at various concentrations. C10 molecules, with the shortest alkyl chain, remained randomly dispersed in the bulk solution and corrosion particles across all concentrations. Despite this random distribution, their high diffusion coefficient suggests strong interactions with corrosion particles. However, this behavior can hinder inhibition efficiency by reducing surface activity and weakening adsorption strength (low adsorption and binding energies). C12 Themolecules exhibited random dispersion at low concentrations (0.04 and 0.08 M) but began to form clusters at 0.12 M. This initial random dispersion favored inhibition efficiency, and the low diffusion coefficient further contributed to enhanced surface activity and stronger adsorption. In contrast, molecules with longer alkyl chains (C14, C16, and C18) formed clusters at all con-

centrations, which is unfavorable for inhibition efficiency. Based on MD simulations, C12 surfactant molecules emerged as the most promising inhibitors, exhibiting a high negative adsorption energy, high binding energy, a low diffusion coefficient, and random dispersion at low concentrations. These computational findings align well with experimental results reported by Gao et al. [7] in 2019, where dodecyl trimethyl ammonium chloride (DTAC) surfactant molecules with a 12-carbon alkyl chain demonstrated the highest inhibition efficiency compared to other surfactants with different chain lengths.

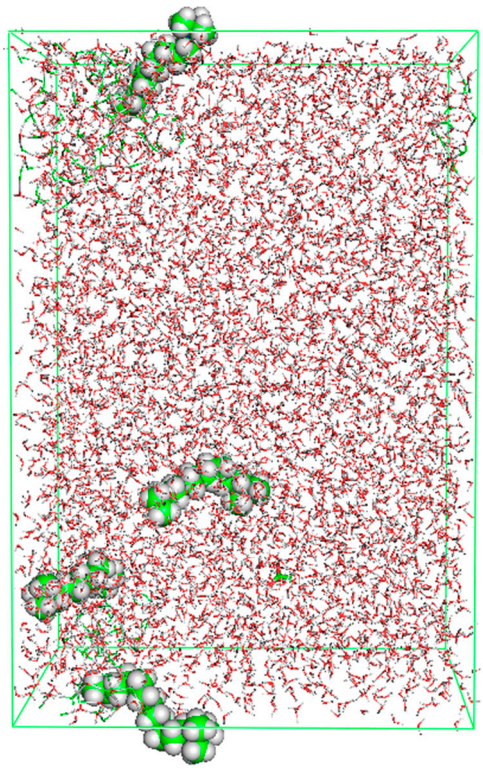

Figure 6. The behavior of CI molecules in 1.0 M HCl and 500 ppm acetic acid at 333 K after simulation (green sphere—carbon atom, white sphere—hydrogen atom, red sphere—oxygen atom, and dark blue sphere—chloride atom).

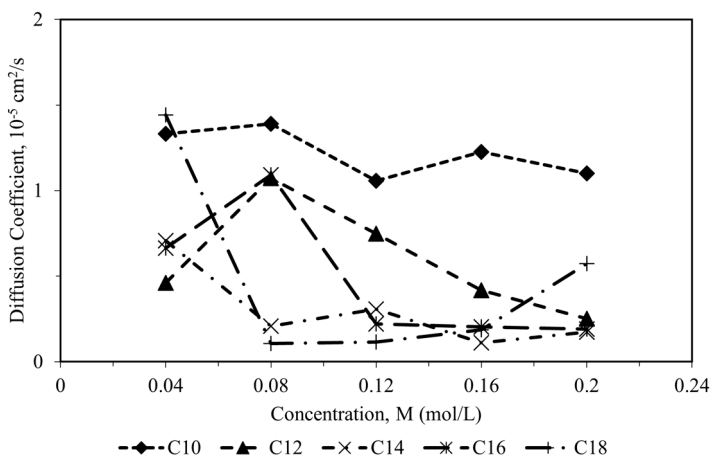

Figure 7. Diffusion coefficients of all CI molecules at different concentrations in the presence of 1.0 M HCl and 500 ppm acetic acid at 333 K calculated via MD simulation.

Table 6. Cluster aggregation of all CI molecules at different concentrations.

CI Molecules	Cluster Aggregation				
	0.04 M	0.08 M	0.12 M	0.16 M	0.20 M
C10	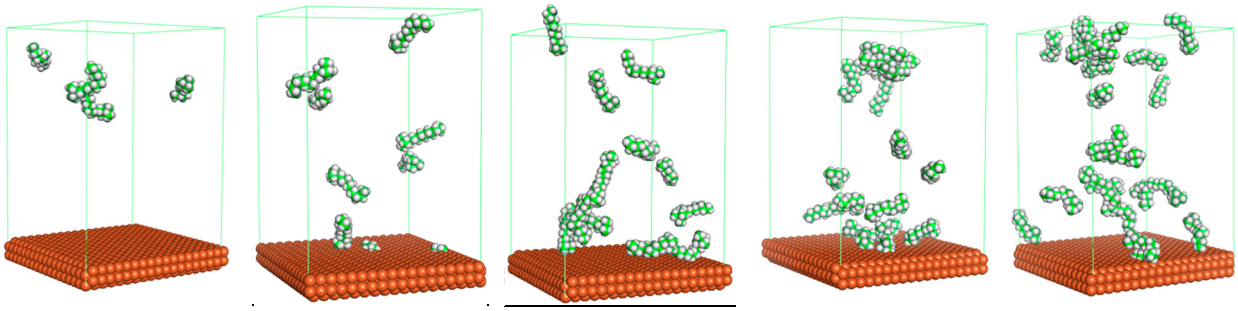				
C12	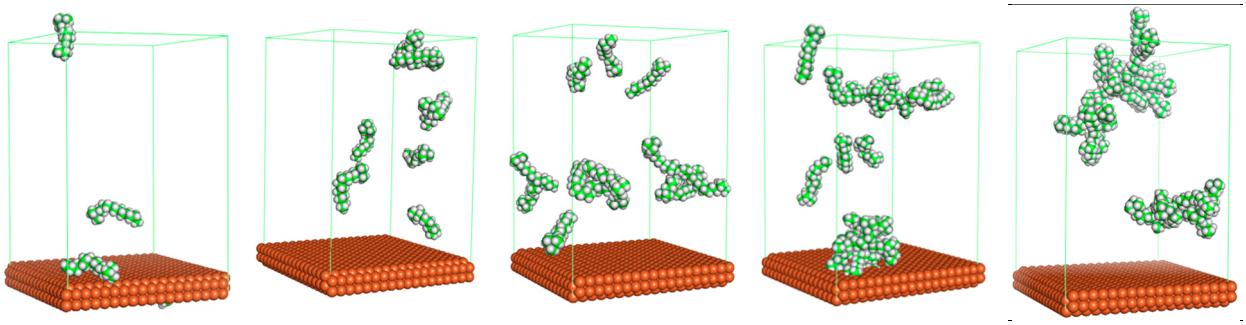				
C14	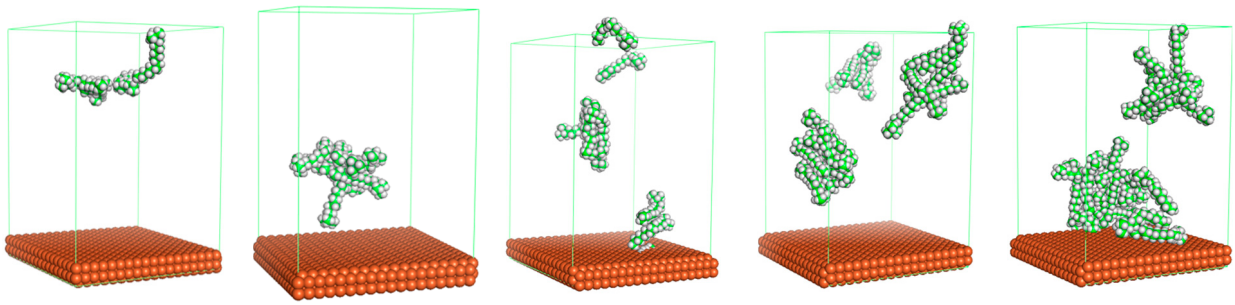				
C16	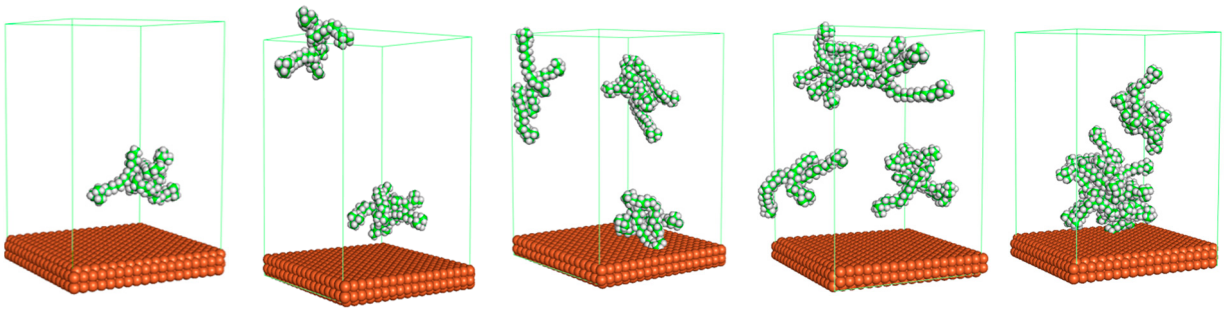				
C18	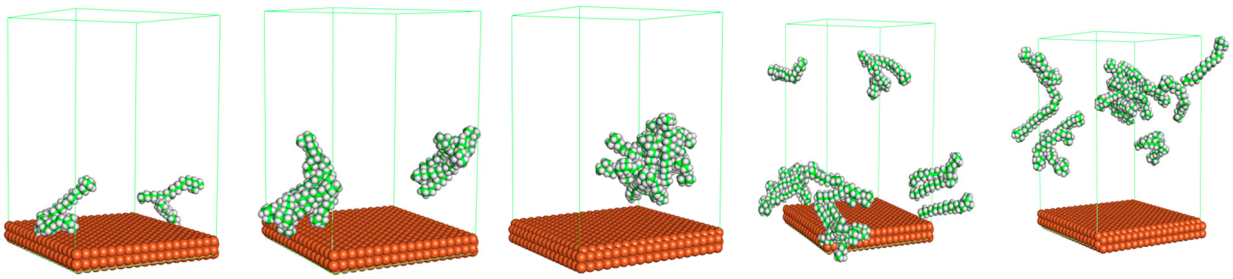				

4. Conclusions

The DFT calculation and MD simulation methods successfully investigated the adsorption properties of all cationic quaternary ammonium surfactants CI molecules with different chain lengths throughout this study. All CI molecules show a high reactive adsorption center with lower band-gap energy at 1.26 eV in the DFT calculation. The region of the reactive adsorption center for all CI molecules is focused on the molecules' ammonium group (N^+). The values of other parameters derived in the DFT calculation also showed the reactive center's ability to donate and accept electrons on the metal surface. The inhibition efficiency ranking for all CI molecules based on adsorption energy and binding energy is as follows: C16 > C12 > C10 > C14 > C18, where C16 had the highest negative value of adsorption energy and the highest binding energy value. However, the C16 molecules formed a cluster even at low concentration in the molecular aggregation analysis. Thus, the C12 ammonium surfactants gave the most promising corrosion inhibitor compared to its significant surfactants with different chain lengths based on the MD simulation method analysis. It showed high adsorption and binding energy after C16 molecules, and it behaved in a randomly scattered form in the molecular aggregation analysis. The excellent agreement between the computer simulation data with the experimental results from the literature and the success in analyzing the inhibition efficiency of all ammonium CI molecules proves the validity of using computer modeling in this application. Therefore, the CI activities and adsorption properties analysis based on computer modeling can be helpful for future reference on the development of a new CI molecule.

Supplementary Materials: The following supporting information can be downloaded at: https://www.mdpi.com/article/10.3390/chemengineering9010007/s1. Tables S1–S5 listed the partial atomic charges for all CI molecules.

Author Contributions: K.J.: conceptualization, resources, funding acquisition, supervision, and project administration. M.S.N.: formal analysis, investigation, and writing—original draft. K.K.E.: conceptualization and resources. A.H.: formal analysis, investigation, and writing—original draft. N.B.: conceptualization and resources. N.M.R.N.M.D.: writing—review and editing. A.M.N.A.: writing—review and editing. F.S.: writing—review and editing. N.N.D.: investigation and writing—review and editing. All authors have read and agreed to the published version of the manuscript.

Funding: This research was funded by the Yayasan Universiti Teknologi Petronas-Fundamental Research Grant (YUTP-FRG), grant number 015LC0-409.

Data Availability Statement: The data will be available upon request.

Acknowledgments: The authors would like to acknowledge Universiti Teknologi PETRONAS for sponsoring this work under Yayasan Universiti Teknologi Petronas-Fundamental Research Grant (YUTP-FRG).

Conflicts of Interest: Author Noorazlenawati Borhan, Nik M. Radi Nik M. Daud, Azmi M. Nor A and Firdaus Suhor were employed by the company PETRONAS Research Sdn Bhd. The remaining authors declare that the research was conducted in the absence of any commercial or financial relationships that could be construed as a potential conflict of interest.

References

1. Zehra, S.; Mobin, M.; Aslam, J. An overview of the corrosion chemistry. In *Environmentally Sustainable Corrosion Inhibitors*; Elsevier: Washington, DC, USA, 2022; pp. 3–23.
2. Chafale, A.; Kapley, A. Biosurfactants as microbial bioactive compounds in microbial enhanced oil recovery. *J. Biotechnol.* **2022**, *352*, 1–15. [CrossRef] [PubMed]
3. Niu, J.; Liu, Q.; Lv, J.; Peng, B. Review on microbial enhanced oil recovery: Mechanisms, modeling and field trials. *J. Petrol. Sci. Eng.* **2020**, *192*, 107350. [CrossRef]

4. Kurapati, Y. A Molecular Dynamics Study to Understand Behavior of Corrosion Inhibitors in Bulk Aqueous Phase and Near Metal-Water Interface. Master's Thesis, Ohio University, Athens, OH, USA, 2018.
5. Xiong, Y.; Cao, M. Application of surfactants in corrosion inhibition of metals. *Curr. Opin. Colloid Interface Sci.* **2024**, *73*, 101830. [CrossRef]
6. Verma, C.; Quraishi, M.A.; Rhee, K.Y. Hydrophilicity and hydrophobicity consideration of organic surfactant compounds: Effect of alkyl chain length on corrosion protection. *Adv. Colloid Interface Sci.* **2022**, *306*, 102723. [CrossRef] [PubMed]
7. Minlan, G.; Lei, F.; Liu, Q.; Zhang, J.; Chen, G. Effect of the alkyl chain of quaternary ammonium cationic surfactants on corrosion inhibition in hydrochloric acid solution. *Comptes Rendus Chim.* **2019**, *22*, 355–362.
8. Deyab, M.A.; Ashmawy, A.M.; Nessim, M.I.; Mohsen, Q. New Gemini surfactants based on alkyl benzenaminium: Synthesis and links to application of corrosion protection. *J. Mol. Liq.* **2021**, *332*, 115855. [CrossRef]
9. Abdellaoui, O.; Skalli, M.K.; Haoudi, A.; Kandri Rodi, Y.; Arrousse, N.; Taleb, M.; Ghibate, R.; Senhaji, O. Study of the inhibition of corrosion of mild steel in a 1M HCl solution by a new quaternary ammonium surfactant. *Moroc. J. Chem.* **2021**, *9*, 44–56.
10. Alnajjar, A.O.; Abd El-Lateef, H.M. A novel approach to investigate the synergistic inhibition effect of nickel phosphate nanoparticles with quaternary ammonium surfactant on the Q235-mild steel corrosion: Surface morphology, electrochemical-computational modeling outlines. *J. Mol. Liq.* **2021**, *337*, 116125. [CrossRef]
11. Numin, M.S.; Hassan, A.; Jumbri, K.; Eng, K.K.; Borhan, N.; Daud, N.M.R.N.M.; Suhor, F.; Wahab, R.A. A recent review on theoretical studies of Gemini surfactant corrosion inhibitors. *J. Mol. Liq.* **2022**, *368*, 120649. [CrossRef]
12. Zhu, H.; Li, X.; Lu, X.; Wang, J.; Hu, Z.; Ma, X. Efficiency of Gemini surfactant containing semi-rigid spacer as microbial corrosion inhibitor for carbon steel in simulated seawater. *Bioelectrochemistry* **2021**, *140*, 107809. [CrossRef] [PubMed]
13. Chen, X.; Chen, Y.; Cui, J.; Li, Y.; Liang, Y.; Cao, G. Molecular dynamics simulation and DFT calculation of "green" scale and corrosion inhibitor. *Comput. Mater. Sci.* **2021**, *188*, 110229. [CrossRef]
14. Becke, A.D. Density-functional theory. III. The role of exact exchange. *J. Chem. Phys.* **1993**, *98*, 5648–5652. [CrossRef]
15. Becke, A.D. Density functional calculations of molecular bond energies. *J. Chem. Phys.* **1986**, *84*, 4524–4529. [CrossRef]
16. Hanwell, M.D.; Curtis, D.E.; Lonie, D.C.; Vandermeersch, T.; Zurek, E.; Hutchison, G.R. Avogadro: An advanced semantic chemical editor, visualization, and analysis platform. *J. Cheminform.* **2012**, *4*, 17. [CrossRef]
17. Steffen, C.; Thomas, K.; Huniar, U.; Hellweg, A.; Rubner, O.; Schroer, A. Schroer. Software news and updates TmoleX—A graphical user interface for TURBOMOLE. *J. Comput. Chem.* **2010**, *31*, 2967–2970. [CrossRef]
18. Obot, I.B.; Macdonald, D.D.; Gasem, Z.M. Density functional theory (DFT) as a powerful tool for designing new organic corrosion inhibitors. Part 1: An overview. *Corros. Sci.* **2015**, *99*, 1–30. [CrossRef]
19. Dewar, M.J.S.; Thiel, W. Ground states of molecules. 38. The MNDO method. Approximations and parameters. *J. Am. Chem. Soc.* **1977**, *99*, 4899–4907. [CrossRef]
20. Pearson, R.G. Absolute electronegativity and hardness: Application to inorganic chemistry. *Inorg. Chem.* **1988**, *27*, 734–740. [CrossRef]
21. Henriquez-Roman, J.H.; Padilla-Campos, L.; Paez, M.A.; Zagal, J.H.; Rubio, M.A.; Rangel, C.M.; Costamagna, J.; Cardenas-Jiron, G. The influence of aniline and its derivatives on the corrosion behaviour of copper in acid solution: A theoretical approach. *J. Mol. Struct. THEOCHEM* **2005**, *757*, 1–7. [CrossRef]
22. Sastri, V.S.; Perumareddi, J.R. Molecular orbital theoretical studies of some organic corrosion inhibitors. *Corros. Sci.* **1997**, *53*, 617–622. [CrossRef]
23. Lukovits, I.; Kalman, E.; Zucchi, F. Corrosion inhibitors—Correlation between electronic structure and efficiency. *Corrosion* **2001**, *57*, 3–8. [CrossRef]
24. Haris, N.I.N.; Sobri, S.; Yusof, Y.N.; Kassim, N.K. An overview of molecular dynamic simulation for corrosion inhibition of ferrous metals. *Metals* **2021**, *11*, 46. [CrossRef]
25. Mazlan, N.; Jumbri, K.; Kassim, M.A.; Wahab, R.A.; Rahman, M.B.A. Density functional theory and molecular dynamics simulation studies of bio-based fatty hydrazide-corrosion inhibitors on Fe (110) in acidic media. *J. Mol. Liq.* **2022**, *347*, 118321. [CrossRef]
26. Essmann, U.; Perera, L.; Berkowitz, M.L.; Darden, T.; Lee, H.; Pedersen, L.G. A smooth particle mesh Ewald method. *J. Chem. Phys.* **1995**, *103*, 8577. [CrossRef]
27. Hess, B. P-LINCS: A parallel linear constraint solver for molecular simulation. *J. Chem. Theory Comput.* **2008**, *4*, 116–122. [CrossRef]
28. Miyamoto, S.; Kollman, P.A. Settle: An analytical version of the SHAKE and RATTLE algorithm for rigid water models. *J. Comput. Chem.* **1992**, *13*, 952–962. [CrossRef]
29. Kokalj, A. On the alleged importance of the molecular electron-donating ability and the HOMO–LUMO gap in corrosion inhibition studies. *Corros. Sci.* **2021**, *180*, 109016. [CrossRef]
30. Ogunyemi, B.T.; Latona, D.F.; Ayinde, A.A.; Adejoro, I.A. Theoretical investigation to corrosion inhibition efficiency of some chloroquine derivatives using density functional theory. *Adv. J. Chem. A* **2020**, *3*, 485–492. [CrossRef]

31. Zhou, X.; Hu, S.; Wang, Y.; Ullah, S.; Hu, J.; Liu, H.; Xu, B. The surface adsorption, aggregate structure and antibacterial activity of Gemini quaternary ammonium surfactants with carboxylic counterions. *R. Soc. Open Sci.* **2019**, *6*, 190378. [CrossRef] [PubMed]
32. Xu, W.; Zhang, B.; Deng, Y.; Yang, L.; Zhang, J. Nitrate on localized corrosion of carbon steel and stainless steel in aqueous solutions. *Electrochim. Acta* **2021**, *369*, 137660. [CrossRef]
33. Pakiet, M.; Tedim, J.; Kowalczyk, I.; Brycki, B. Functionalised novel Gemini surfactants as corrosion inhibitors for mild steel in 50 mM NaCl: Experimental and theoretical insights. *Colloids Surf. A* **2019**, *580*, 123699. [CrossRef]
34. Wang, J.; Hou, B.; Xiang, J.; Chen, X.; Gu, T.; Liu, H. The performance and mechanism of bifunctional biocide sodium pyrithione against sulfate reducing bacteria in X80 carbon steel corrosion. *Corros. Sci.* **2019**, *150*, 296–308. [CrossRef]
35. Verma, C.; Ebenso, E.E.; Quraishi, M.A. Molecular structural aspects of organic corrosion inhibitors: Influence of -CN and -NO_2 substituents on designing of potential corrosion inhibitors for aqueous media. *J. Mol. Liq.* **2020**, *316*, 113874. [CrossRef]
36. Tazouti, A.; Errahmany, N.; Rbaa, M.; Galai, M.; Rouifi, Z.; Touir, R.; Zarrouk, A.; Kaya, S.; Touhami, M.E.; Ibrahimi, B.E.; et al. Effect of hydrocarbon chain length for acid corrosion inhibition of mild steel by three 8-(n-bromo-R-alkoxy)quinoline derivatives: Experimental and theoretical investigations. *J. Mol. Struct.* **2021**, *1244*, 130976. [CrossRef]
37. Abdallah, M.; Guesmi, N.E.; Al-Gorair, A.S.; El-Sayed, R.; Meshabi, A.; Sobhi, M. Enhancing the anticorrosion performance of mild steel in sulfuric acid using synthetic non-ionic surfactants: Practical and theoretical studies. *Green Chem. Lett. Rev.* **2021**, *14*, 382–394. [CrossRef]
38. Defrawy, A.E.; Abdallah, M.; Al-Fahemi, J. Electrochemical and theoretical investigation for some pyrazolone derivatives as inhibitors for the corrosion of c-steel in 0.5 M hydrochloric acid. *J. Mol. Liq.* **2019**, *288*, 110994. [CrossRef]
39. Hameed, R.S.A.; Al-Bagawi, A.H.; Shehata, A.H.; Shamroukh, A.H.; Abdallah, M. Corrosion inhibition and adsorption properties of some heterocyclic derivatives on C-steel surface in HCl. *J. Bio Tribo Corros.* **2020**, *6*, 51.
40. Alfakeer, M.; Abdallah, M.; Fawzy, A. Corrosion Inhibition effect of expired ampicillin and flucloxacillin drugs for mild steel in aqueous acidic medium. *Int. J. Electrochem. Sci.* **2020**, *15*, 3283–3297. [CrossRef]
41. Boulechfar, C.; Ferkous, H.; Delimi, A.; Berredjem, M.; Kahlouche, A.; Madaci, A.; Djellali, S.; Boufas, S.; Djedouani, A.; Errachid, A.; et al. Corrosion inhibition of Schiff base and their metal complexes with [Mn (II), Co (II) and Zn (II)]: Experimental and quantum chemical studies. *J. Mol. Liq.* **2023**, *378*, 121637. [CrossRef]
42. Wang, L.; Wang, H.; Seyeux, A.; Zanna, S.; Pailleret, A.; Nesic, S.; Marcus, P. Adsorption mechanism of quaternary ammonium corrosion inhibitor on carbon steel surface using ToF-SIMS and XPS. *Corros. Sci.* **2023**, *213*, 110952. [CrossRef]
43. Haque, J.; Mazumder, M.A.J.; Quraishi, M.A.; Ali, S.A.; Aljeaban, N.A. Pyrrolidine-based quaternary ammonium salts containing propargyl and hydrophobic C-12 and C-16 alkyl chains as corrosion inhibitors in aqueous acidic media. *J. Mol. Liq.* **2020**, *320*, 114473. [CrossRef]
44. Mubarak, G.; Verma, C.; Mazumder, M.A.J.; Barsoum, I.; Alfantazi, A. Corrosion inhibition of P110 carbon steel useful for casing and tubing applications in 3.5% NaCl solution using quaternary ammonium-based copolymers. *J. Mol. Liq.* **2024**, *402*, 124691. [CrossRef]
45. Babarao, R.; Jiang, J. Diffusion and separation of CO_2 and CH_4 in silicalite, C168 Schwarzite, and IRMOF-1: A comparative study from molecular dynamics simulation. *Langmuir* **2008**, *24*, 5474–5484. [CrossRef] [PubMed]
46. Garrido, L.; Pozuelo, J.; Lopez-Gonzalez, M.; Fang, J.; Riande, E. Simulation and experimental studies on proton diffusion in polyelectrolytes based on sulfonated naphthalenic copolyimides. *Macromolecules* **2009**, *42*, 6572–6580. [CrossRef]
47. Obot, I.B.; Bahraq, A.A.; Alamri, A.H. Density functional theory and molecular dynamics simulation of the corrosive particle diffusion in pyrimidine and its derivatives films. *Comput. Mater. Sci.* **2022**, *210*, 111428. [CrossRef]
48. Goyal, M.; Vashisht, H.; Alrefaee, S.H.; Jain, R.; Kumar, S.; Kaya, S.; Guo, L.; Verma, C. Decyltriphenylphosphonium bromide containing hydrophobic alkyl chain as a potential corrosion inhibitor for mild steel in sulfuric acid: Theoretical and experimental studies. *J. Mol. Liq.* **2021**, *336*, 116166. [CrossRef]
49. Sharma, S.; Ko, X.; Kurapati, Y.; Singh, H.; Nesic, S. Adsorption Behavior of organic corrosion inhibitors on metal surfaces—Some new insights from molecular simulations. *Corrosion* **2019**, *75*, 90–105. [CrossRef] [PubMed]